Chem Rev Lett 7 (2024) 661-676

Research Article

Chemical Review and Letters
journal homepage: www.chemrevlett.com
ISSN (online): 2645-4947 (print) 2676-7279

Characterization of tetramethyl guanidinium 4-nitro phenoxide (TMG-NP) and tetraphenyl guanidinium 4-nitro phenoxide (TPG-NP) as new ionic liquids (ILs) using DFT and *ab initio*

Rafid Kamal Jameel[1], Hayder Hamid Abbas Al-Anbari[2], Aseel Salah Mansoor[3], Usama Kadem Radi[4], Ameer Hasan Kadhem[5], Hala Bahair[6], Farnaz Behmagham[7,] *, Vahideh Abbasi[8]

[1]*Al-Noor University College, Iraq*
[2]*Ahl Al bayt University, College of pharmacy, Kerbala, Iraq*
[3]*Gilgamesh Ahliya University, Baghdad, Iraq*
[4]*usamakadem@nust.edu.iq Collage of Pharmacy, National University of Science and Technology, Dhi Qar, 64001, Iraq*
[5]*Al-Zahrawi University College, Karbala, Iraq*
[6]*Medical technical college, Al-Farahidi University, Iraq*
[7]*Department of Chemistry, Miandoab University, Islamic Azad University, Miandoab, Iran*
[8]*Department of Chemistry, University of Zanjan, Zanjan, Iran*

ARTICLE INFO

Article history:
Received 30 June 2024
Received in revised form 30 August 2024
Accepted 30 August 2024
Available online 23 September 2024

Keywords:
ILs,
TPG-NP,
TMG-NP,
ωb97xd,
HF.

ABSTRACT

Here, we have been evaluated the geometrical, electronic and spectroscopic characters of **TMG-NP** and **TPG-NP**, at DFT *vs. ab initio*. Assessment of these ILs have been done *via* the optimized structures using B3PW91, ωb97xd and HF/6-311++G(d,p). The spectral analysis of both ILs is containing IR, Raman, ^{1}H NMR,^{13}C NMR, and UV–Vis. Both **TMG-NP** & **TPG-NP** with high polarizability, hyperpolarizability (β_{tot}) and polarity are proposed as molecules with high NLO character. These characters are comparable with those of the related standards to urea structure. The calculated β_{tot} values for **TMG-NP**, especially **TPG-NP** structure are found to be about 31.5 - 45.5 times greater than the β_{tot} value of urea, leading us to consider these structures as the suitable candidates for NLO materials. Both systems display differentially *E*g (band gap), global reactivity, charge delocalization and DOS plot that are realized *via* NBO analysis. The electron density transfers from the electropositive atoms to the electronegative atoms, because of electronegative difference of them that is recognized *via* MEP analysis. Less stability and more reactivity of **TPG-NP** than **TMG-NP** arising from less hyperconjugation, more π-stacking and more steric effect of **TPG-NP** than **TMG-NP**. Finally, in order to reduction in friction along with wear, **TPG-NP** with higher nucleophilicity and lower electrophilicity than **TMG-NP**, is suggested as better noncorrosive lubricant additive for tribological performance.

1. Introduction

Owing to the distinctive features of the IL salts; *e.g.* melting point below 100 °C, high chemical stability, high thermal stability, negligible vapor pressure, ordinary polarity, and so on; they are recommended for applications such as reaction surroundings, extractants, catalysts, lubricants, lubricant additives to a variety of base oils, *etc.* [1-8]. Even though, the development of ILs benefits from imidazolium or pyridinium cations and halide anions, they are prone to hydrolysis and generate hazardous as well as corrosive hypohalous acids [9]. For steel-steel contact benefitting base fluid of PEG (polyethylene

∗ Corresponding author; e-mail: behmagham.farnaz99@gmail.com, behmagham_farnaz@yahoo.com
https://doi.org/10.22034/crl.2024.465452.1368

glycol), these salts are revealed the tribological properties, anti-wear and friction reduction [10,11]. Furthermore, the amino acids due to the carboxylic and amine groups, can act as both cationic and anionic counter ions in the synthesis of task-specific ILs for diverse applications [12-14]. Recently, some of amino acids and alkylguanidines successfully synthesized and characterized using FT-IR along with NMR data [15]. Now, we are investigated **TMG-NP** and **TPG-NP** as the designed ILs *via* computational chemistry (Figure 1).

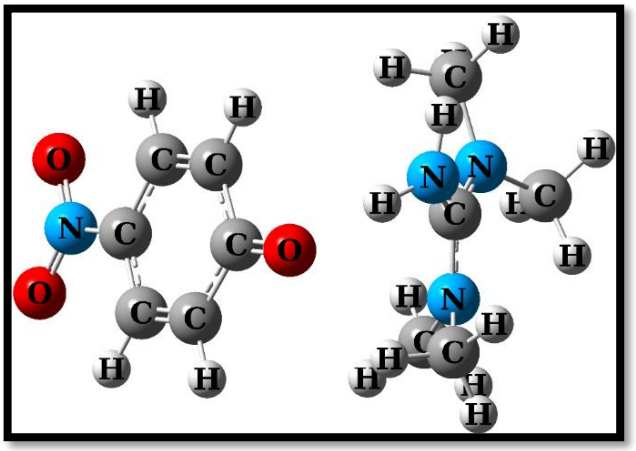

TMG-NP

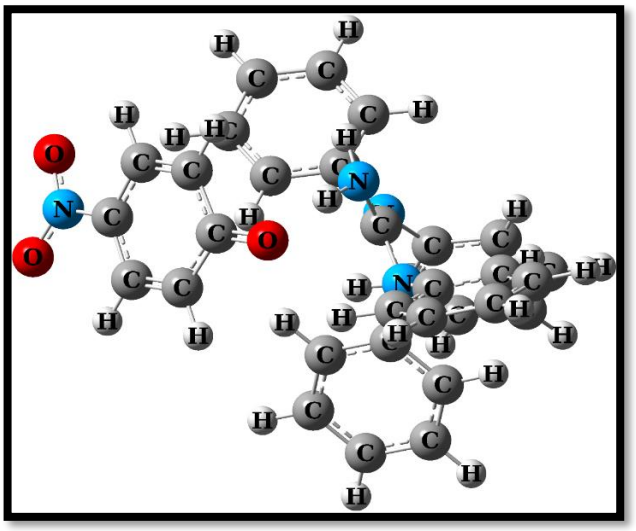

TPG-NP

Fig. 1. The optimized structures of **TMG-NP** and **TPG-NP**, at ωb97xd/6-311++G(d,p).

2. Computational methods

The structures of **TMG-NP** and **TPG-NP** are optimized and the theoretical data are achieved using the GAMMES [16] package at B3PW91/6-311++G** [17], ωb97xd/6-311++G** [18], and HF/6-311++G** [19]; which are advantageous for diffuse functions (Scheme 1) [20-22].

Moreover, the υ_{min} calculations are done to approve the optimized structures to be an energy minimum (and not a transition state) also to acquire vibrational spectra [23]. The vibrational IR & Raman spectra of the scrutinized ILs are calculated in the harmonic approximation. Here, in order to understand the microscopic origin of nonlinear behavior of the scrutinized ILs, we are investigated total static dipole moment (μ_0), isotropic polarizability (α) and first hyperpolarizability (β) tensor for them, at the selected methods. First hyper-polarizability is a third rank tensor which can be illustrated by a 3*3*3 matrix [24]. To find the total hyperpolarizability (β_{tot}), we are calculated all components of this matrix as β_{xxx}, β_{xxy}, β_{xyy}, β_{yyy}, β_{xxz}, β_{xyz}, β_{yyz}, β_{xzz}, β_{yzz}, and β_{zzz}, using ωb97xd/6-311++G(d,p) and HF/6-311++G(d,p).

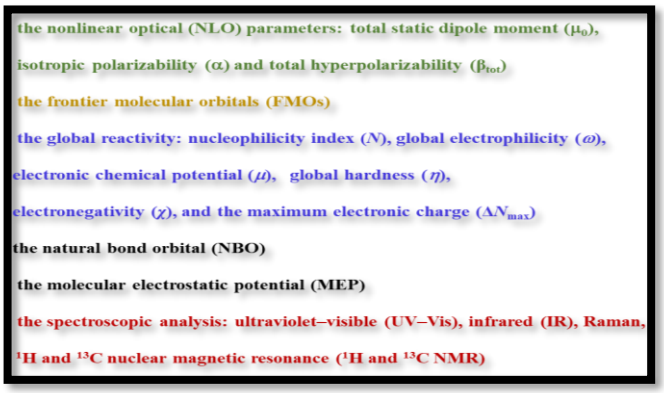

Scheme 1. The studied acronyms in this research.

Utilizing the x, y and z Cartesian coordinate, we are expected μ_0, α, β_{tot} parameters *via* the succeeding equations: $\mu_0 = (\mu^2_x + \mu^2_y + \mu^2 z)^{1/2}$; $\alpha = 1/3\ (\alpha_{xx} + \alpha_{yy} + \alpha_{zz})$; $\beta_{tot} = [(\beta_{xxx} + \beta_{xyy} + \beta_{xzz})^2 + (\beta_{yyy} + \beta_{yzz} + \beta_{yxx})^2 + (\beta_{zzz} + \beta_{zxx} + \beta_{zyy})^2]^{1/2}$ and also $\beta_{tot} = (\beta^2_x + \beta^2_y + \beta^2_z)^{½}$ [25]. The TD-DFT technique is operated to obtain UV–Vis spectrum. The optimized structures are used in the isotropic chemical shifts, FMO, NBO, and MEP analysis [26]. The chemical shifts of ^{1}H & ^{13}C NMR spectra are calculated *via* gauge-independent atomic orbitals in chloroform solvent [27]. The global reactivity is distinguished through the succeeding expressions: $N = E_{HOMO(Nu)} - E_{HOMO(TCNE)}$; $\omega = \mu^2 / 2\eta$; $\mu = (E_{HOMO} + E_{LUMO}) / 2$; $\eta = (E_{LUMO} - E_{HOMO}) / 2$; $\chi = -\mu$; $S = 1 / \eta$, and $\Delta N_{max} = -\mu / \eta$ [28].

3. Results and Discussion

3.1. Geometry

The geometrical data of the designed ILs are found *via* the method modification (Tables S1 and S2). Both ILs show a non-planar geometry (with C_1 symmetry) and bond length between single bond and double bond of two carbon atoms in the 4-nitro phenoxide moiety; in the range of 1.378 - 1.434 and 1.375 – 1.433 Å at ωb97xd, 1.367 - 1.430 and 1.366 - 1.432 Å at HF for **TMG-NP** and **TPG-NP**, correspondingly. Also, both ILs show an intra-molecular hydrogen bond between the corresponding cationic and anionic moieties (N-H…..O; See Graphical Abstract); in the bond length of 1.537, 1.661 Å at ωb97xd, 1.603 and 1.778 Å at HF for **TMG-NP** and **TPG-NP**, respectively. The ∠CCC values in the NP rings of **TMG-NP** and **TPG-NP** are changed from 115.94º to 121.99º, and from 116.13º to 121.89º at ωb97xd; also from 115.88º to 121.91º, and from 115.85º to 121.19º at HF, correspondingly. In comparison to benzene structure which it's ∠CCC value supports the sp^2 hybrid of 120º, now the studied ILs are confirmed sp^2 hybridization for their carbon atoms with ∠CCC values lower and/or higher than 120º in the corresponding NP cycles. The smaller ∠CCC bond angle than 120º in NP ring of the scrutinized ILs, exhibits that the related carbon atoms have more p character than normal sp^2 in C=C and/or C=O bonds. Furthermore, the theoretical data display similar range of C=N bond lengths in 1.438 Å at ωb97xd, 1.425 Å at HF for **TMG-NP**; 1.434 Å at ωb97xd and 1.423 Å at HF for **TPG-NP** showing good delocalization of $2p_\pi$-electrons among nitro group and phenoxide ring. Also, the corresponding torsion angle is found about 177.347º at ωb97xd, 178.518º at HF for **TMG-NP**; 175.491º at ωb97xd and 178.667º at HF for **TPG-NP** that implies these moieties are in the same plane.

3.2. Harmonic vibrations

Here, no imaginary frequency mode is found for the studied ILs; henceforth both structures are emerged as a true minimum on their potential energy surfaces. Moreover, the IR & Raman spectra of two species are compared and contrasted at ωb97xd/6-311++G(d,p) and HF/6-311++G(d,p) (Figure 2).

The calculations show both **TMG-NP** and **TPG-NP** structures with non-planar geometry; 36 and 64 atoms; 102 and 186 active normal vibrational modes in their corresponding IR & Raman spectra, respectively, in which the most important peaks are discussed, now. For instance, the strongest stretching frequency of N_{29}-H_{30} bond in **TMG-NP** structure is calculated as 2419.47 and 3055.73 cm^{-1} at ωb97xd and HF, respectively; while the stretching frequency of N_{29}-H_{31} bond in **TMG-NP** structure is calculated as 3689.44 and 3878.24 cm^{-1} at ωb97xd and HF, respectively.

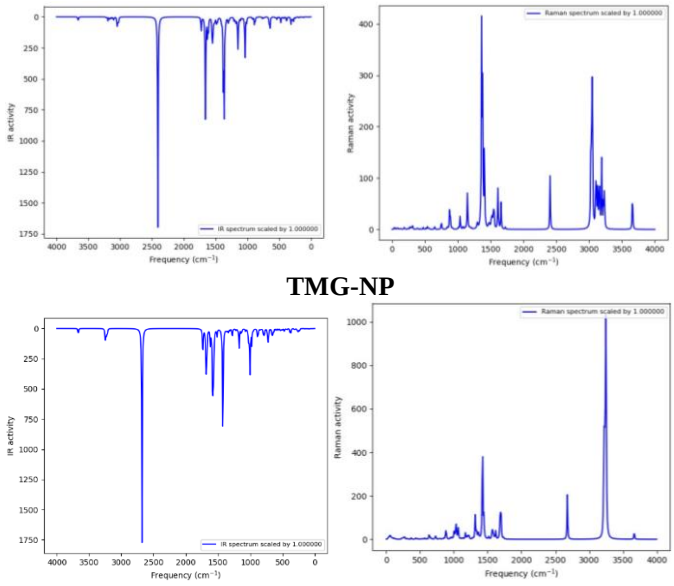

Fig. 2. The vibration frequencies of **TMG-NP** and **TPG-NP** in IR and Raman spectra using at ωb97xd/6-311++G(d,p).

We are obtained wave numbers of N_{29}-H_{30} bond in IR & Raman spectrum of **TMG-NP** structure in the region of 1836.87 and 105.63 cm^{-1} at ωb97xd; 1533.34 and 147.43 cm^{-1} at HF, while the wave numbers of N_{29}-H_{31} bond in **TMG-NP** structure is obtained in the region of 46.24 and 77.99 cm^{-1} at ωb97xd; 59.88 and 47.85 cm^{-1} at HF, respectively. Clearly, H_{30} atom *via* H—bonding is absorbed to O_6 atom of 4-nitro phenoxide and then it is repulsed from O_6 atom. The C=O stretching vibrations usually are reported in the range of 1000–1300 cm^{-1}. In this research, 4-nitro phenolic C_2=O_6 stretching vibrations of **TMG-NP** structure are observed in the region of 1363.78 and 1405.28 cm^{-1}, at ωb97xd; 1487.53 and 1664.61 cm^{-1}, at HF. The strongest stretching frequency of N_{13}-H_{14} bond in **TPG-NP** structure is observed in 2678.14 and 3347.38 cm^{-1} at ωb97xd and HF, respectively; while the stretching frequency of N_{13}-H_{15} bond in **TPG-NP** structure is considered in 3667.31 and 3878.08 cm^{-1} at ωb97xd and HF, respectively. The wave numbers of N_{13}-H_{14} bond in IR & Raman spectra of **TPG-NP** structure are obtained in the region of 1816.06 and 209.73 cm^{-1} at ωb97xd; 964.33 and 126.85 cm^{-1} at HF, while the wave numbers of N_{13}-H_{15} bond in this structure are found in the region of 55.43 and 40.33 cm^{-1} at ωb97xd; 60.49 and 40.83 cm^{-1} at HF, respectively. As above mentioned, H_{14} atom of **TPG-NP** *via* H—bonding is absorbed to its O_6 atom and then is repulsed from this atom. Also, 4-nitro phenolic C_2=O_6 stretching vibrations of **TPG-NP** structure are calculated in the region of 1444.00 and 1618.88 cm^{-1} at ωb97xd; 1530.13 and 1711.83 cm^{-1} at HF. There are some vibrational frequencies in the range of 1300–1700 cm^{-1} for C–C, N–C, C–O, N–O, N–H starching and bending bond in aromatic compounds. The C=O stretching vibrations of **TMG-NP** ring are observed in the region of 804.05 and 44.90 cm^{-1} at ωb97xd; 1307.64 and 160.68 cm^{-1} at HF in IR spectrum; while it's corresponding signals in Raman spectrum are appeared at 405.48 and 174.98 cm^{-1} at ωb97xd; 513.06 and 53.50 cm^{-1} at HF. Here, the C=O stretching vibrations of **TPG-NP** ring are studied in the region of 30.83 and 124.43 cm^{-1} at ωb97xd; 220.84 and 210.55 cm^{-1} at HF in IR spectrum; while it's corresponding signals in Raman spectrum are emerged at 95.74 and 37.68 cm^{-1} at ωb97xd; 434.28 and 55.58 cm^{-1} at HF.

3.3. Nonlinear optical properties

The μ_0 value of **TMG-NP** structure is estimated about 12.00 – 15.00 Debye, while the μ_0 value of **TPG-NP** structure is calculated about 13.00 – 17.00 Debye, at ωb97xd/6-311++G(d,p) and HF/6-311++G(d,p) (Table 1).

In continuous, we are found α values of **TMG-NP** and **TPG-NP** structures between 23.66×10^{-24} - 25.58×10^{-24} esu and 53.47×10^{-24} - 56.28×10^{-24} esu, respectively, at HF/6-311++G(d,p) and ωb97xd/6-311++G(d,p). Also, we are considered β_{tot} values of **TMG-NP** and **TPG-NP** structures in the range of $1.93 \times 10^{-30} – 2.76 \times 10^{-30}$ esu and $4.09 \times 10^{-30} – 6.43 \times 10^{-30}$ esu, at ωb97xd/6-311++G(d,p) and HF/6-311++G(d,p), respectively.

Table 1. The NLOs of **TMG-NP** and **TPG-NP**, at the selected methods.

Parameter	TMG-NP		TPG-NP	
	ωb97xd	**HF**	**ωb97xd**	**HF**
μ_x (Debye)	-10.97	-14.49	-11.47	-15.97
μ_y (Debye)	3.74	3.74	6.32	5.75
μ_z (Debye)	1.97	1.73	-1.36	-1.28
μ_0 (Debye)	11.76	15.07	13.17	17.02
α_{xx} (*u.a.*)	200.43	179.69	466.07	442.87
α_{yy} (*u.a.*)	186.20	166.06	361.41	336.64
α_{zz} (*u.a.*)	150.80	151.22	354.85	343.82
α (*u.a.*)	179.14	165.66	394.11	374.44
$\alpha \times 10^{-24}$ (esu)	25.58	23.66	56.28	53.47
β_{xxx} (*u.a.*)	-161.01	-230.84	-387.33	-673.81
β_{xyy} (*u.a.*)	-32.38	-50.14	-45.54	-22.70
β_{xzz} (*u.a.*)	-25.89	-37.13	-20.59	-40.26
β_x (*u.a.*)	-219.28	-318.12	-453.47	-736.77
β_{yyy} (*u.a.*)	45.49	41.07	43.00	19.23
β_{yxx} (*u.a.*)	-20.49	-29.54	29.81	40.41
β_{yzz} (*u.a.*)	14.60	17.99	43.65	21.88
β_y (*u.a.*)	39.60	29.52	116.47	81.52
β_{zzz} (*u.a.*)	9.71	4.58	30.17	42.72
β_{zxx} (*u.a.*)	-25.74	-26.34	-106.91	-82.77
β_{zyy} (*u.a.*)	26.69	25.78	6.28	-29.23
β_z (*u.a.*)	10.66	4.02	-70.46	-69.27
$\beta^2_x+\beta^2_y+\beta^2_z$	49765.06	102086.70	224167.10	554280.11
β_{tot} (*u.a.*)	223.08	319.51	473.46	744.50
$\beta_{tot} \times 10^{-30}$ (esu)	1.93	2.76	4.09	6.43

Hence, we propose both ILs as an interesting NLO material, so that **TPG-NP** species is more reactive for dipole–dipole interaction than **TMG-NP** species. Urea as a reference species is chosen to investigation of the NLO character. It is respected generally as a threshold value for comparative goals. The β_{tot} values for **TMG-NP** and especially **TPG-NP** structure are established to be about 31.5 -45.5 times greater than the β_{tot} value of urea (0.3728×10^{-30} esu), leading us to suggest **TMG-NP** and especially **TPG-NP** structure as the suitable candidate for NLO materials.

3.4. ^{1}H & ^{13}C NMR spectra

The chemical shifts of ILs are studied in chloroform solvent (Tables 2 and 3).

Firstly, both ILs structures are confirmed by assignment of their^{1} H NMR spectrum, which reveals relative intensities of the aromatic and aliphatic proton resonances. One wide signal is appeared in 12.03 and 10.85 ppm as the most deshield peak in aromatic area for NH proton (N_{29}-H_{30} bond) of **TMG-NP** structure, while other proton (N_{29}-H_{31} bond) is appeared in 3.25 and 3.27 ppm using ωb97xd and HF, respectively. The signals in aromatic area are found for H_4, H_5, H_{35}, and H_{36} of **NP** moiety in **TMG-NP** structure in the range of 7.98 – 5.43 ppm using ωb97xd; 8.41 – 5.34 ppm using HF. One singlet signal in aliphatic area for CH_3 protons of **TMG-NP** structure is appeared in the range of 1.15 – 2.90 ppm using ωb97xd; 1.66 – 2.73 ppm using HF. Furthermore, the signals in aromatic area are found for H_4, H_5, H_{63}, and H_{64} of **NP** moiety in **TPG-NP** structure in the range of 8.39 – 7.61 ppm using ωb97xd; 8.88 – 7.24 ppm using HF.

Table 2. The ^{1}H NMR chemical shifts of **TMG-NP** and **TPG-NP** structures in chloroform.

Atom	ωb97xd	HF	Atom	ωb97xd	HF
	TMG-NP			**TPG-NP**	
30	12.03	10.85	**14**	11.50	9.92
4	7.98	8.41	**58**	9.61	9.35
5	7.77	8.36	**4**	8.39	8.88
35	6.13	5.90	**5**	8.17	8.45
36	5.43	5.34	**63**	7.91	8.58
26	3.68	3.95	**64**	7.61	7.24
31	3.25	3.27	**25,61,62**	7.45	7.67
16	2.90	2.73	**50,40,28,60,56**	7.25	7.47
28	2.32	2.46	**38**	7.00	7.47
14	2.42	2.37	**51**	6.92	7.47
18	2.42	2.37	**34**	6.75	7.09
20	2.21	2.27	**27,47,49**	6.44	7.01
22	1.83	2.09	**45**	5.77	6.29
15	2.32	2.09	**36**	5.69	6.42
23	1.53	2.09	**23**	5.58	6.91
19	2.11	2.09	**15**	4.14	5.42
27	1.88	1.92	**29**	6.92	7.78
24	1.15	1.66	**39**	5.77	7.16

Table 3. The ^{13}C NMR chemical shifts of **TMG-NP** and **TPG-NP** structures in chloroform.

Atom	ωb97xd	HF	Atom	ωb97xd	HF
	TMG-NP			**TPG-NP**	
2	182.92	190.10	**2**	185.19	191.16
10	171.02	177.36	**10**	169.21	180.18
1	137.11	142.14	**41,19,52**	149.48	150.31
3	133.59	142.09	**30**	145.23	147.25
8	132.69	129.74	**54**	142.01	143.88
9	122.57	116.66	**3,1**	138.88	142.90
7	116.99	113.30	**35**	136.78	138.97
21	38.52	37.30	**20,43,57,22,37,59**	135.56	137.79
25	37.95	37.02	**26,32,33,46,48**	133.64	136.65
17	36.90	36.82	**21,44,24,31**	132.74	135.21
13	35.85	34.68	**53,55**	131.45	134.19
			8,9	130.77	133.29
			7	124.16	129.21

One signal in aromatic area for C_{54}-H_{58} proton of **TPG-NP** structure is appeared in 9.61 and 9.35 ppm using ωb97xd and HF, respectively. Clearly, this proton is oriented in 2.321 Å from oxygen atom of phenoxide moiety. Other signals in aromatic area is appeared for protons of tetraphenyl groups in this structure in the range of 7.45 – 5.77 ppm using ωb97xd; 7.67 – 6.29 ppm using HF. The ^{13}C chemical shifts are displayed signals in aliphatic area for C_{13}, C_{17}, C_{21}, and C_{25} of **TMG-NP** structure in the range of 35.85 - 38.52 ppm using ωb97xd; 34.68 - 37.30 ppm using HF. Furthermore, the ^{13}C chemical shifts of both ILs are displayed signals in aromatic area for other carbon atoms of **TMG-NP** structure and all carbon atoms of **TPG-NP** structure in the range of 116.99 - 182.92 and 124.16 - 185.19 ppm using ωb97xd; 113.30 - 190.10 and 129.21 - 191.16 ppm using HF, correspondingly.

3.5. FMOs, Reactivity & UV–Vis

After extensive computations, we found helpful information regarding to the FMO energies, shapes, *E*g, reactivity, kinetic stability and spectral data of various compounds and nanostructures [29-35]. Accordingly, in this section, we are probed FMOs, reactivity and UV–Vis of ILs using the used methods. the calculated FMOs of **TMG-NP** with 68 HOMOs from 198 MOs are

introduced HOMO and LUMO with -0.2539 and 0.0253 *a.u.* at ωb97xd, while the corresponding values are appeared with -0.2556 and 0.1185 *a.u.* at HF. The HOMO coefficients of **TMG-NP** are delocalized over it's **TMG** moiety, while the HOMO coefficients of **TPG-NP** are delocalized over both TPG and NP moieties (Figure 3).

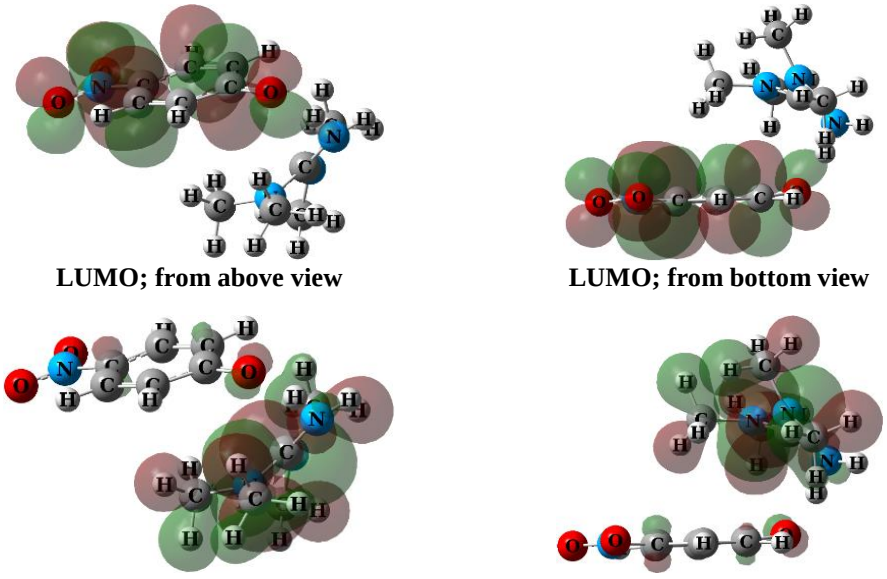

LUMO; from above view **LUMO; from bottom view**

HOMO; from above view **HOMO; from bottom view**

Fig. 3. The selected FMOs of **TMG-NP**, at ωb97xd/6-311++G(d,p).

Accordingly, the LUMO coefficients of **TMG-NP** are delocalized over it's **NP** moiety, while the LUMO coefficients of **TPG-NP** are delocalized over both TPG and NP moieties. These observations confirm more band gap of **TMG-NP** for electron donation from HOMO to LUMO than **TPG-NP** (Figure 4).

The band gap values of the **TMG-NP** and **TPG-NP** structures are estimated 4.43 and 4.40 eV using B3PW91; 7.60 and 7.28 eV using ωb97xd; 10.18 and 9.27 eV using HF, respectively (Tables 4, 5 and Figure 5).

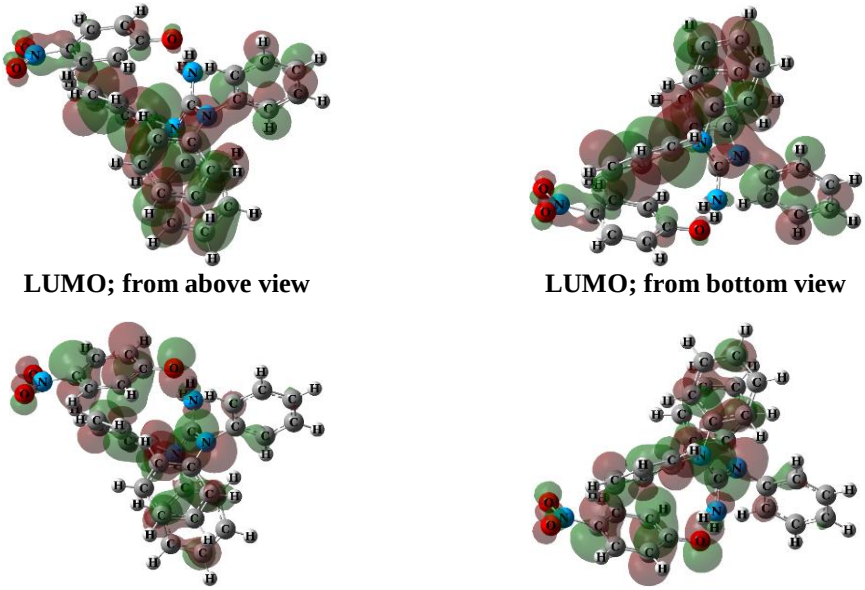

LUMO; from above view **LUMO; from bottom view**

HOMO; from above view **HOMO; from bottom view**

Fig. 4. The selected FMOs of **TPG-NP**, at ωb97xd/6-311++G(d,p).

Table 4. The FMO energies, and *E*g of **TMG-NP** and **TPG-NP** using the used methods.

Method	HOMO (*a.u.*)	LUMO (*a.u.*)	*E*g (eV)	ΔN_{max} (eV)
TMG-NP				
B3PW91	-0.2224	-0.0597	4.43	1.73
ωb97xd	-0.2539	0.0253	7.60	0.82
HF	-0.2556	0.1185	10.18	0.37
TPG-NP				
B3PW91	-0.2185	-0.0568	4.40	1.70
ωb97xd	-0.2505	0.0170	7.28	0.87
HF	-0.2501	0.0905	9.27	0.47

Table 5. The calculated *N*, μ, η, ω, χ, *S* and ΔN_{max} of **TMG-NP** and **TPG-NP** using the used methods.

Method	*N* (eV)	μ (eV)	η (eV)	ω (eV)	*S* (eV)	ΔN_{max} (eV)
TMG-NP						
B3PW91	3.41	-3.84	2.21	3.33	0.45	1.73
ωb97xd	2.55	-3.11	3.80	1.27	0.26	0.82
HF	2.50	-1.86	5.09	0.34	0.20	0.37
TPG-NP						
B3PW91	3.51	-3.75	2.20	3.19	0.45	1.70
ωb97xd	2.64	-3.18	3.64	1.39	0.27	0.87
HF	2.66	-2.17	4.63	0.51	0.22	0.47

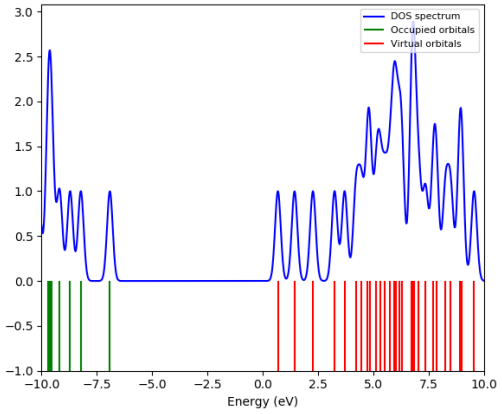

TMG-NP

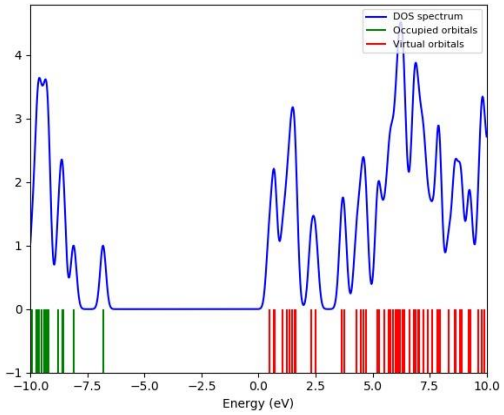

TPG-NP

Fig. 5. The DOS plots of **TMG-NP** and **TPG-NP**, at ωb97xd/6-311++G(d,p).

Reactivity factors of **TMG-NP** and **TPG-NP** structures are estimated as *N*: 3.41 and 3.51 eV using B3PW91; 2.55 and 2.64 eV using ωb97xd; 2.50 and 2.66 eV using HF, μ: -3.84 and -3.75 eV using B3PW91; -3.11 and -3.18 eV using ωb97xd; -1.86 and -2.17 eV using HF, η: 2.21 and 2.20 eV using B3PW91; 3.80 and 3.64 eV using ωb97xd; 5.09 and 4.63 eV using HF, ω: 3.33 and 3.19 eV using B3PW91; 1.27 and 1.39 eV using ωb97xd; 0.34 and 0.51 eV using HF, along with ΔN_{max}: 1.73 and 1.70 eV using B3PW91; 0.82 and 0.87 eV using ωb97xd; 0.37 and 0.47 eV using HF, correspondingly. Therefore, **TPG-NP** with lower band gap, higher *N* than **TMG-NP** is suggested as good noncorrosive lubricant additive for tribological performance.

The absorption UV–Vis spectra of both ILs are analyzed *via* the main molecular orbital contributions, λ_{max}, *E*, *f*, *T* and *T*% (Scheme 1, Figure 6 and Tables 6, 7).

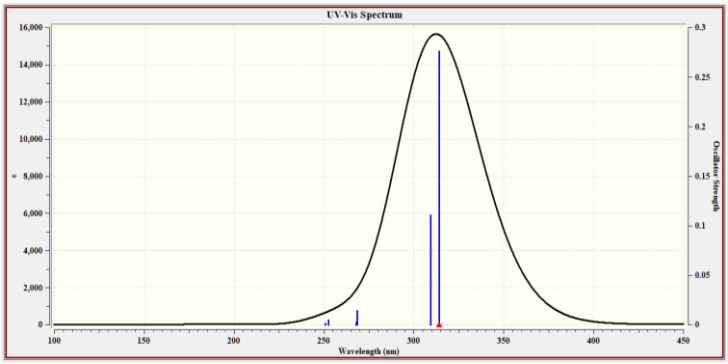

TMG-NP

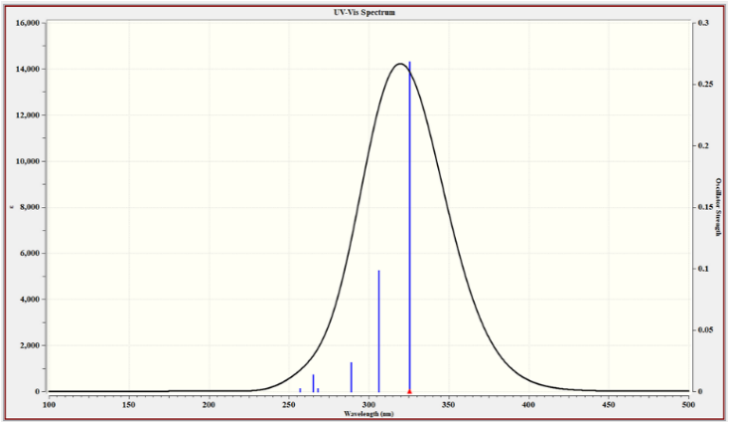

TPG-NP

Fig. 6. The UV–Vis spectrum of **TMG-NP** and **TPG-NP**, at ωb97xd/6-311++G(d,p).

Table 6. The main molecular orbital contributions, λ_{max}, and *E* using the selected methods.

Method	MO	Number	λ_{max} (nm)	*E* (ev)
		TMG-NP		
ωb97xd	HOMO → LUMO	68 → 69	313.97	3.95
HF	HOMO → LUMO	68 → 78	260.55	4.76
		TMG-TNP		
ωb97xd	HOMO → LUMO	132 → 133	325.35	3.81
HF	HOMO → LUMO	132 → 150	263.03	4.71

Table 7. The main molecular orbital contributions, *f*, *T*, and *T*% using the selected methods.

Method	MO	*f*	*T*	*T*%
	TMG-NP			
ωb97xd	HOMO → LUMO	0.276	0.589	69.42
HF	HOMO → LUMO	0.483	0.551	52.82
	TMG-TNP			
ωb97xd	HOMO → LUMO	0.268	0.532	56.60
HF	HOMO → LUMO	0.557	0.563	63.46

The calculated absorption maximum of **TMG-NP** and **TPG-NP** structures is appeared as λ_{max}: 313.97 and 325.35 nm, *E:* 3.95 and 3.81 eV, *f*: 0.276 and 0.268 eV, *T*: 0.589 and 0.532, *T*%: 69.42 and 56.60 using ωb97xd; λ_{max}: 260.55 and 263.03 nm, *E:* 4.76 and 4.71 eV, *f*: 0.483 and 0.557 eV, *T*: 0.551 and 0.563, *T*%: 52.82 and 63.46 using HF, correspondingly. Based on these theoretical investigations the long wave length bands are assigned to $n_{\text{O atom of C=O group}} \rightarrow \sigma^*_{\text{N29-H30}}$ and $_{\text{C=O group}} \rightarrow \sigma^*_{\text{N13-H14}}$ bond transitions caused by HOMO-LUMO intramolecular charge transfer from the **TMG** and **TPG** fragments to the corresponding **NP** moiety, correspondingly; while these transitions are not happened for their corresponding $\sigma^*_{\text{N29-H31}}$ and $\sigma^*_{\text{N13-H15}}$ bonds.

3.6. NBO & MEP

NBO analysis of the surveyed ILs is included as a concise of electron donor orbitals, electron acceptor orbitals, and the interaction stabilization energy $E(^2)$ in kcal/mol (Table 8) [29-35].

The principal intramolecular interaction or charge transfer of **TMG-NP** and **TPG-NP** structures is obtained owing to the orbital overlap of lone pairs of oxygen atom to anti-bonding sigma bond. The $E(^2)$ of LP (1) $_{O6} \rightarrow \sigma^*_{(H30–N29)}$, LP (2) $_{O6} \rightarrow \sigma^*_{(H30–N29)}$, and LP (3) $_{O6} \rightarrow \sigma^*_{(H30–N29)}$ is found 9.06, 32.92, and 15.35 kcal/mol using ωb97xd; 8.24, 17.49, and 15.16 kcal/mol using HF, respectively; from unit **1** (**NP**) to unit **2** (**TMG**) of **TMG-NP**. The order of $E(^2)$ is arranged as LP (2) $_{O6} \rightarrow \sigma^*_{(H30–N29)}$ > LP (3) $_{O6} \rightarrow \sigma^*_{(H30–N29)}$ > LP (1) $_{O6} \rightarrow \sigma^*_{(H30–N29)}$. Also, the $E(^2)$ of LP (1) $_{O6} \rightarrow \sigma^*_{(H14–N13)}$, LP (2) $_{O6} \rightarrow \sigma^*_{(H14–N13)}$, and LP (3) $_{O6} \rightarrow \sigma^*_{(H14–N13)}$ is found 8.31, 20.54, and 20.43 kcal/mol using ωb97xd; 5.86, 13.29, and 10.44 kcal/mol using HF, respectively; from unit **1** (**NP**) to unit **2** (**TPG**) of **TPG-NP**. The order of $E(^2)$ is arranged as LP (2) $_{O6} \rightarrow \sigma^*_{(H14–N13)}$ > LP (3) $_{O6} \rightarrow \sigma^*_{(H14–N13)}$ > LP (1) $_{O6} \rightarrow \sigma^*_{(H14–N13)}$. The most stabilization energy is considered for LP (2) $_{O6} \rightarrow \sigma^*_{(H30–N29)}$ in **TMG-NP** and the least stabilization energy is found for LP (1) $_{O6} \rightarrow \sigma^*_{(H14–N13)}$ in **TPG-NP**, at the used methods. This phenomenon is supported *via* the NBO charge; with the aim of charge transformation between the phenoxide oxygen (O_6) and the NH proton in $H_{30}–N_{29}$ bond of **TMG-NP**; and also between the phenoxide oxygen (O_6) and the NH proton in $H_{14}–N_{13}$ bond of **TPG-NP** structure.

Table 8. The selected NBO analysis of **TMG-NP** and **TPG-NP**: electron donor orbital (i), electron acceptor orbital (j), $E(^2)$, and the second-order perturbation theory.

Donor NBO (i)	Acceptor NBO (j)	$E(^2)$	E(j - i) (*a.u.*)	F(i,j) (*a.u.*)
TMG-NP at ωb97xd				
LP (1) O_6	BD*(1) $H_{30} – N_{29}$	9.06	1.09	0.091
LP (2) O_6	BD*(1) $H_{30} – N_{29}$	32.92	0.81	0.146
LP (3) O_6	BD*(1) $H_{30} – N_{29}$	15.35	0.83	0.103
TMG-NP at HF				
LP (1) O_6	BD*(1) $H_{30} – N_{29}$	8.24	1.47	0.099
LP (2) O_6	BD*(1) $H_{30} – N_{29}$	17.49	1.11	0.124
LP (3) O_6	BD*(1) $H_{30} – N_{29}$	15.16	0.97	0.115
TPG-NP at ωb97xd				
LP (1) O_6	BD*(1) $H_{14} – N_{13}$	8.31	1.12	0.088
LP (2) O_6	BD*(1) $H_{14} – N_{13}$	20.54	0.79	0.114
LP (3) O_6	BD*(1) $H_{14} – N_{13}$	20.43	0.71	0.115
TPG-NP at HF				
LP (1) O_6	BD*(1) $H_{14} – N_{13}$	5.86	1.51	0.084
LP (2) O_6	BD*(1) $H_{14} – N_{13}$	13.29	1.08	0.108
LP (3) O_6	BD*(1) $H_{14} – N_{13}$	10.44	0.98	0.069

Hence, we are detected the distributed negative and positive atomic charges of –0.781, +0.456 and -0.803, +0.461 at ωb97xd; -0.892, +0.482 and -0.908, +0.497 at HF, on accepting moiety (O_6 atom) and donating moiety (either H_{30} or H_{14} atom) correspondingly. In addition, it is found less negative and less positive charge transfer in **TMG-NP** than **TPG-NP** (Figures 7 and 8).

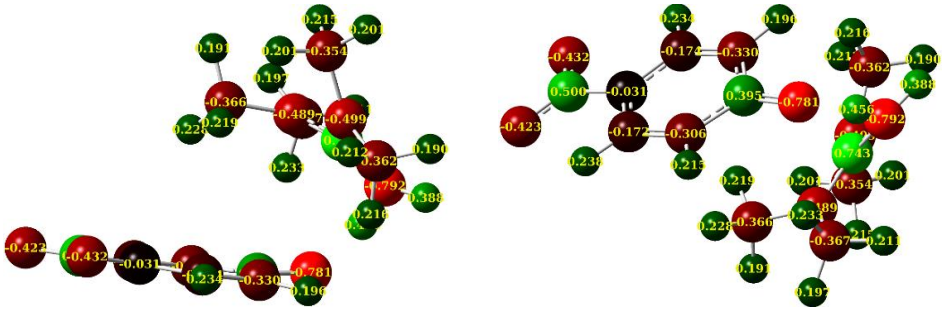

From bottom view **From above view**

Fig. 7. The NBO charge of **TMG-NP**, at ωb97xd/6-311++G(d,p).

The MEP maps of these ILs are recommended as a beneficial character for characterization of electrophilic and nucleophilic sites in the range of -2.000e-3 to +2.000e-3. The red and blue colors reveal the highest negative and positive regions making the suitable sites for electrophilic and nucleophilic attack, independently (Figures 9 and 10).

Henceforth, the most significant interaction of **TMG-NP** and **TPG-NP** structures is characterized on oxygen atoms of 4-nitro phenoxide ($NP^–$) as good electrophilic site and nitrogen atoms of tetramethyl guanidinium (TMG^+) and tetraphenyl guanidinium (TPG^+) as good nucleophilic site with other nucleophile and electrophile sites in lubricants or their surrounding's molecules, correspondingly.

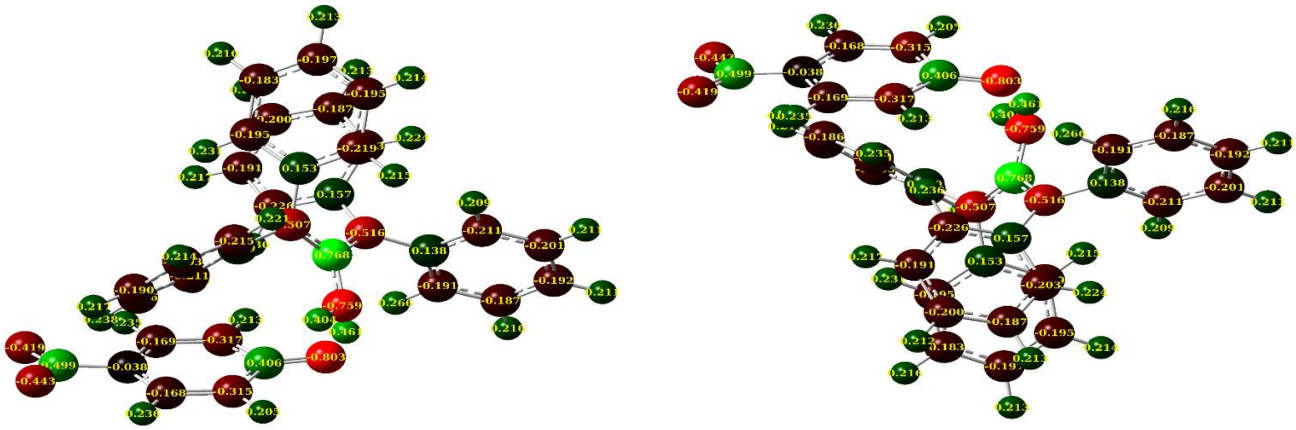

From bottom view **From above view**

Fig. 8. The NBO charge of **TPG-NP**, at ωb97xd/6-311++G(d,p).

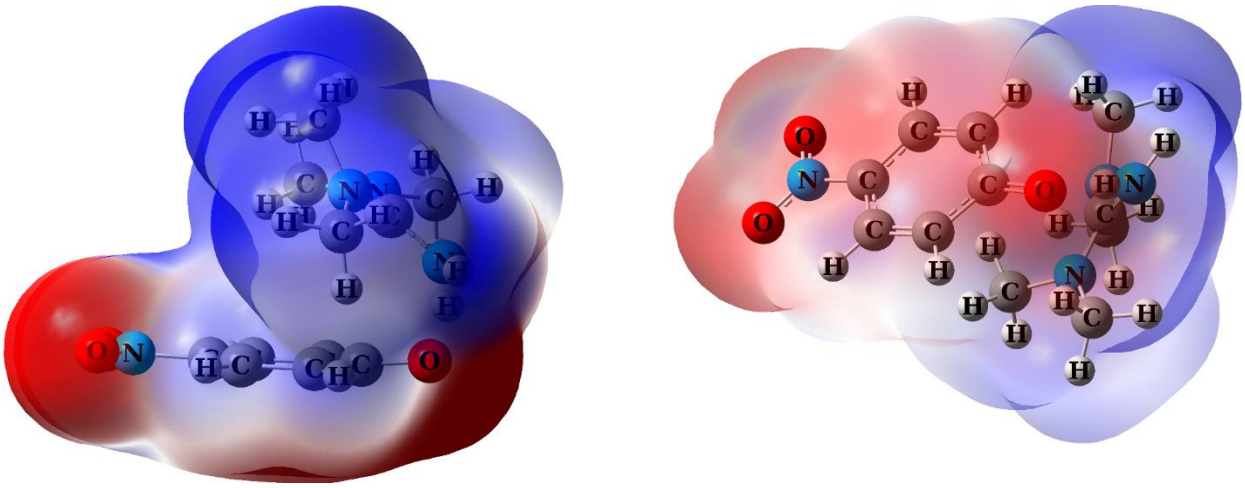

From bottom view **From above view**

Fig. 9. The MEP of **TMG**-NP in the range of -2.000e-3 to +2.000e-3, at ωb97xd/6-311++G(d,p).

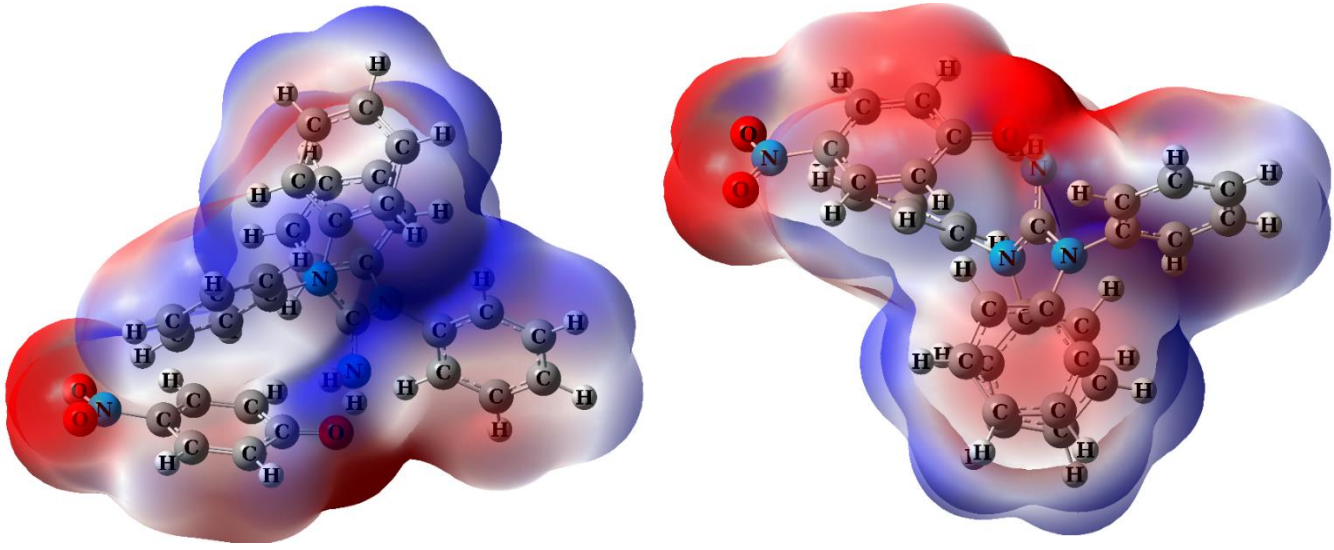

From bottom view **From above view**

Fig. 10. The MEP of **TPG-NP** in the range of -2.000e-3 to +2.000e-3, at ωb97xd/6-311++G(d,p).

4. Conclusion

The design, theoretical analysis and description of ILs based on nitro phenoxide are presented using DFT and *ab initio*. The geometry, frequency, IR, Raman, UV–Vis spectrum, FMO, E_g, DOS global reactivity, NBO and MEP analysis of novel **TMG-NP** and **TPG-NP** structures are identified using ωb97xd/6-311++G(d,p) and HF/6-311++G(d,p). Both **TMG-NP** and **TPG-NP** with high μ_0, α, β_{tot} are introduced as molecules with high NLO character. These characters are comparable with those of the reported standards for urea. The calculated β_{tot} values for **TMG-NP** and especially **TPG-NP** structure are found to be about 31.5 - 45.5 times greater than the β_{tot} value of urea, leading us to consider **TMG-NP** and especially **TPG-NP** structure as the suitable candidates for NLO materials. Both systems display differentially *E*g, DOS, global reactivity, and charge delocalization that is realized *via* NBO analysis. Less stability and more reactivity of **TPG-NP** than **TMG-NP** arising from less hyperconjugation, more π-stacking and more steric effect in **TPG-NP** than **TMG-NP**. Also, **TPG-NP** with higher *N* and lower ω than **TMG-NP** is suggested as better noncorrosive lubricant additive for tribological performance in order to reduction in friction along with wear. As a result, because of different orientation of the bonded hydrogen atoms to nitrogen atoms of TMG^+ (H_{30}–N_{29} and H_{31}–N_{29}) as well as TPG^+ (H_{14}–N_{13} and H_{15}–N_{13}) ions relation to oxygen atoms in carbonyl group of NP^- (C_2=O_6), DFT and *ab initio* calculations cannot provide consistency between vibrational frequencies, spectroscopic data, NBO analysis, *etc*. In this survey, we compared and contrasted DFT *vs. ab initio* methods without experimental observations in order to predict the stability, electronic along with spectroscopic properties of the designed ionic liquids. Our investigation confirmed the ωb97xd method as the best and most reliable theoretical method with 6-311++G(d,p) basis set. Both **TMG-NP** and **TPG-NP** systems are shown higher polarizability, higher hyperpolarizability, and higher polarity (about 31.5 - 45.5 times) than urea, leading us to consider these systems as better candidate for NLO materials. Henceforth, we recommend that the researchers can benefit from this method to evaluate their desired ionic liquid systems before the synthesize procedure; for the sake of time, energy and cost saving.

Acknowledgements

Authors state that no fund is used in this research.

Conflicts of interest

There is not conflict of interest.

References

[1] Z. Lei, B. Chen, Y.-M. Koo, D. R. MacFarlane, Introduction: Ionic Liquids, Chem. Rev. 117 (2017) 6633-6635.

[2] M. Brehm, M. Pulst, J. Kressler, D. Sebastiani, Triazolium-Based Ionic Liquids – A Novel Class of Cellulose Solvents, J. Phys. Chem. B 12318 (2019) 3994-4003.

[3] C.F. Poole, S.K. Poole, Extraction of organic compounds with room temperature ionic liquids, J. Chromatogr. A 1217 (2010) 2268-2286.

[4] P. Karthikeyan, S. A. Aswar, P. N. Muskawar, S. K. Sythana, P. R. Bhagat, S. S. Kumar, P. S. Satvat, A novel l-amino acid ionic liquid for quick and highly efficient synthesis of oxime derivatives - an environmental benign approach, Arab. J. Chem. 9 (2016) S1036- S1039.

[5] S. Esfahani, J. Akbari, S. Soleimani-Amiri, Novel ionic liquid systems based on three-nitro phenoxide: spectroscopic and electronic characterization via theoretical and experimental study, Main Group Chem. 23 (2024) 1-15.

[6] S. Yang, J.S.S. Wong, F. Zhou, Ionic Liquid Additives for Mixed and Elastohydrodynamic Lubrication, Tribol. Trans. 61 (2018) 816-826.

[7] G. Huwang, Q. Yu, Z. Ma, M. Cai, F. Zhou, W. Liu, Oil-soluble ionic liquids as antiwear and extreme pressure additives in poly-α-olefin for steel/steel contacts, Friction 7 (2019) 18-31.

[8] C. Verma, D. K. Verma, E. E. Ebenso, M. A. Quraishi, Sulfur and phosphorus heteroatom-containing compounds as corrosion inhibitors: An overview, Heteroatom Chem. 29 (2018) e21437.

[9] P.M. Amorim, A.M. Ferraria, R. Colaço, L.C. Branco, B. Saramago, Imidazolium-based ionic liquids used as additives in the nanolubrication of silicon surfaces, Beilstein J. Nanotechnol. 8 (2017)1961-1971.

[10] M. Yao, Y. Liang, Y. Xia, F. Zhou, Bisimidazolium Ionic Liquids as the High-Performance Antiwear Additives in Poly(ethylene glycol) for Steel−Steel Contacts, ACS Appl. Mater. Interfaces 1 (2009) 467-471.

[11] M. S. Raja Shahrom, C. D. Wilfred, F. K. Chong, Synthesis and characterization of Poly[VBTMA]Ala, AIP Conf. Proc. 1621 (2014) 237–243.

[12] S. Yue, X.-J. Hao, P.-P. Wang, J. Li, Amino acid-based ionic liquids for CO2 conversion to form cyclic carbonate under solvent-free conditions, Mol. Catal. 433 (2017) 420-429.

[13] J. Hua, Y. Shi, Non-corrosive Green Lubricant with Dissolved Lignin in Ionic Liquids Behave as Ideal

Lubricants for Steel-DLC Applications, Front. Chem. 7 (2019) 857.

[14] C. Jiang, W. Li, J. Nian, W. Lou, X. Wang, Tribological evaluation of environmentally friendly ionic liquids derived from renewable biomaterials, Friction 2018, 6, 208-218.

[15] A. M. Sadanandan, P. K. Khatri, R.C. Saxena, S. L. Jain, Guanidine based amino acid derived task specific ionic liquids as noncorrosive lubricant additives for tribological performance, J. Mol. Liq. 313 (2020) 113527.

[16] (a) M. W. Schmidt, K. K. Baldridge, J. A. Boatz, S. T. Elbert, M. S. Gordon, J. H. Jensen, S. Koseki, N. Matsunaga, K. A. Nguyen, S. J. Su, T. L. Windus, M. Dupuis, J. A. Montgomery, General atomic and molecular electronic structure system, J. Comput. Chem. 14 (11) (1993) 1347-1363. (b) A. L. Sobolewski, W. Domcke, Ab Initio Investigation of the Structure and Spectroscopy of Hydronium−Water Clusters, J. Phys. Chem. A 106 (2002) 4158–4167.

[17] (a) J. P. Perdew, Y. Wang, Accurate and simple analytic representation of the electron-gas correlation energy, Phys. Rev. B 45 (1992) 13244-13249. (b) J.P. Perdew, K. Burke, M. Ernzerhof, Generalized Gradient Approximation Made Simple, Phys. Rev. Lett. 78 (1997) 1396–1396.

[18] J. -D. Chai, M. Head-Gordon, Long-range corrected hybrid density functionals with damped atom–atom dispersion corrections, Phys. Chem. Chem. Phys. 10 (2008) 6615-6620.

[19] P. Pulay, G. Fogarasi, F. Pang, J.E. Boggs, Systematic ab initio gradient calculation of molecular geometries, force constants, and dipole moment derivatives, J. Am. Chem. Soc. 101 (1979) 2550-2560.

[20] (a) P. C. Hariharan, J. A. Pople, Accuracy of AH, equilibrium geometries by single determinant molecular orbital theory. J. Mod. Phys. 27 (1974) 209-214. (b) M. M. Francl, W. J. Pietro, W. J. Hehre, J. S. Binkley, M. S. Gordon, D. J. DeFrees, J. A. Pople, Self-Consistent Molecular Orbital Methods. XXIII. A Polarization-Type Basis Set for Second Row Elements, J. Chem. Phys. 77 (1982) 3654-3665. (c) T. Clark, J. Chandrasekhar, G. W. Spitznagel, P.v.R. Schleyer, Efficient diffuse function-augmented basis sets for Anion Calculations. III. The 3-21+G set for first-row elements, Li-F, J. Comput. Chem. 4 (1983) 294-301. (d) M. J. Frisch, J. A. Pople, J. S. Binkley, Self-Consistent Molecular Orbital Methods 25: Supplementary Functions for Gaussian Basis Sets, J. Chem. Phys. 80 (1984) 3265-3269.

[21] (a) W. J. Hehre, L. Radom, P. v. R. Schleyer, J. A. Pople, *Ab Initio* Molecular Orbital Theory, John Wiley & Sons, New York (1986). (b) J. B. Foresman, A. Frisch, Exploring Chemistry with Electronic Structure Methods, Gaussian, Inc., Pittsburgh. PA (1996). (c) R. A. Kendall, T. H. Jr. Dunning, R. J. Harrison, Electron affinities of the first-row atoms revisited. Systematic basis sets and wave functions. J. Chem. Phys. 96 (1992) 6796-6806. (d) R. Krishna, M. J. Frisch, J. A. Pople, Contribution of Triple Substitutions to the Electron Correlation Energy in Fourth Order Perturbation Theory. J. Chem. Phys. 72 (1980) 4244-4246.

[22] A.P. Scott, L. Radom, Harmonic Vibrational Frequencies: An Evaluation of Hartree−Fock, Møller−Plesset, Quadratic Configuration Interaction, Density Functional Theory, and Semiempirical Scale Factors, J. Phys. Chem. 100 (1996) 16502-16513.

[23] (a) C. Sosa, J. Andzelm, B.C. Elkin, E. Wimmer, K.D. Dobbs, D.A. Dixon, A local density functional study of the structure and vibrational frequencies of molecular transition-metal compounds, J. Phys. Chem. 96 (1992) 6630-6636. (b) Foresman JB, Frisch AE, Exploring Chemistry with Electronic Structure Methods. 3rd ed. (Wallingford, CT: Gaussian (2015).

[24] R. Rahmani, N. Boukabcha, A. Chouaih, F. Hamzaoui, S. Goumri-Said, On the molecular structure, vibrational spectra, HOMO-LUMO, molecular electrostatic potential, UV–Vis, first order hyperpolarizability, and thermodynamic investigations of 3-(4-chlorophenyl)-1-(1yridine-3-yl) prop-2-en-1-one by quantum chemistry calculations, J. Mol. Struct. 1155 (2018) 484-495.

[25] R. Jawaria, M. Hussain, M. Khalid, M. U. Khan, M. N. Tahir, M. M. Naseer, A. A. C. Braga, Z. Shafiq, Synthesis, crystal structure analysis, spectral characterization and nonlinear optical exploration of potent thiosemicarbazones based compounds: A DFT refine experimental study, Inorganic. Chim. Acta 486 (2019) 162-171.

[26] (a) F. Weinhold, E. D. Glendening, NBO 7.0 Program Manual Natural Bond Orbital Analysis Programs. J. Comput. Chem. 33 (2012) 2363-2379. (b) E. D. Glendening, C. R. Landis, F. Weinhold, Natural bond orbital methods. Wiley Interdiscip. Rev. Comput. Mol. Sci. 2 (2012) 1-42. (c) G. Zhang, C. B. Musgrave, Comparison of DFT Methods for Molecular Orbital Eigenvalue Calculations. J. Phys. Chem. A 111 (2007) 1554-61.

[27] G. Schreckenbach, T. Ziegler, Calculation of NMR shielding tensors based on density functional theory and a scalar relativistic Pauli-type Hamiltonian. The application to transition metal complexes Int. J. Qua. Chem. 1997, 61, 899-918.

[28] (a) L. R. Domingo, E. Chamorro, P. Pérez, Understanding the Reactivity of Captodative Ethylenes in Polar Cycloaddition Reactions. A Theoretical Study. J. Org. Chem. 73 (2008) 4615-4624. (b) R. G. Parr, L. Szentpaly, S. Liu, Electrophilicity Index. J. Am. Chem. Soc. 121 (1999) 1922-1924. (c) R. G. Pearson Absolute electronegativity and hardness: applications to organic chemistry. J. Org. Chem. 54 (1989) 1423-1430. (d) P. K. Chattaraj, S. Giri, Stability, Reactivity, and Aromaticity of Compounds of a Multivalent Superatom. J. Phys. Chem. A 111 (2007) 11116-11121. (e) J. Padmanabhan, R. Parthasarathi, V. Subramanian, P. K. Chattaraj, Electrophilicity-Based Charge Transfer Descriptor. J. Phys. Chem. A 111 (2007) 1358-1361.

[29] (a) M. Afshar, R. Ranjineh Khojasteh, R. Ahmadi, M. Nakhaei Moghaddam, In silico adsorption of lomustin anticancer drug on the surface of boron nitride nanotube, Chem. Rev. Lett. 4(3) (2021) 178-184. (b) B. Hashemzadeh, L. Edjlali, P. Delir Kheirollahi Nezhad, E. Vessally, A DFT studies on a potential anode compound for Li-ion batteries: Hexa-cata-hexabenzocoronene nanographen, Chem. Rev. Lett. 4(4) (2021) 232-238. (c) N. Salehi, E. Vessally, l. Edjlali, I. Alkorta, M. Eshaghi, Nan@ Tetracyanoethylene (n= 1-4) systems: Sodium salt vs Sodium electride, Chem. Rev. Lett. 3 (2020) 207-217. (d) M. Kamel, K. Mohammadifard, Thermodynamic and reactivity descriptors Studies on the interaction of Flutamide anticancer drug with nucleobases: A computational view, Chem. Rev. Lett. 4(1) (2021) 54-65.

[30] (a) M. Vakili, V. Bahramzadeh, M. Vakili, A comparative study of SCN-adsorption on the Al12N12, Al12P12, and Si and Ge-doped Al12N12 nano-cages to remove from the environment, J. Chem. Lett. 1(4) (2020) 172-178. (b) M. Mosavi, Adsorption behavior of mephentermine on the pristine and Si, Al, Ga-doped boron nitride nanosheets: DFT studies, J. Chem. Lett. 1 (2020) 164-171.

(c) E. Vessally, S.A. Siadati, A. Hosseinian, L. Edjlali, Selective sensing of ozone and the chemically active gaseous species of the troposphere by using the C20 fullerene and graphene segment, Talanta 162 (2017) 505-510. (d) S.A. Siadati, E. Vessally, A. Hosseinian, L. Edjlali, Possibility of sensing, adsorbing, and destructing the Tabun-2D-skeletal (Tabun nerve agent) by C20 fullerene and its boron and nitrogen doped derivatives, Synt. Met. 220 (2016) 606-611.

[31] (a) S. Arshadi, F. Abdolahzadeh, E. Vessally, Butadiyne-linked porphyrin nanoring as a highly selective O2 gas sensor: A fast response hybrid sensor, J. Mol. Graph. Model. 119 (2023) 108371. (b) M. Khalif, S. Daneshmehr, S. Arshadi, İ. Söğütlü, E.A. Mahmood, V. Abbasi, E. Vessally, Adsorption of O2 molecule on the transition metals (TM (II)= Sc2+, Ti2+, V2+, Cr2+, Mn2+, Fe2+, Co2+, Ni2+, Cu2+ and Zn2+) porphyrins induced carbon nanocone (TM (II) PCNC), J. Mol. Graph. Model. 119 (2023) 108362. (c) M. Ghaghaei, M. Babazadeh, F. Behmagham, L. Edjlali, E. Vessally, A theoretical evaluation for new fused remote N-heterocyclic silylenes (RNHSis) using density functional theory, J. Phys.Org. Chem. (2023) e4475. (d) S. Azimi, B. Mohammadi, S. Babadoust, E. Vessally, In Silico study and design of some new potent threonine tyrosine kinase inhibitors using molecular docking simulation, Mol. Simulat. (2023) 1-8.

[32] (a) I. S. Hasan, A. A. Majhool, M. H. Sami, M. Adil, S. S. S. A. Azziz, DFT Investigation of structure, stability, NBO charge on Titanium—Nitrogen nanoheterofullerenes evolved from a small nanocage, Chem. Rev. Lett. 6 (2023), 10.22034/crl.2023.392371.1223.

(b) A. A. Muhammad, U. Umar, Adsorption of SO2 and NO2 on ZrO2 (1 1 0) Surface: Density Functional Theory and Molecular Dynamic Simulation Studies, J. Chem. Lett. 3 (2022) 135-143. 10.22034/jchemlett.2023.363900.1088. (c) M. Mosavi, Theoretical study of interaction between Mexiletine drug and pristine, Si-, Ga- and Al-doped boron nitride nano sheet, J. Chem. Lett. 3 (2022) 150-158. 10.22034/jchemlett.2023.384082.1103. (d) A. Karbakhshzadeh, S. Majedi, V. Abbasi, Computational investigation on interaction between graphene nanostructure BC3 and Rimantadine drug: Possible sensing study of BC3 and its doped derivatives on Rimantadine, J. Chem. Lett. 3 (2022) 108-113. 10.22034/jchemlett.2022.352857.1079.

[33] (a) A. Ajala, A. Uzairu, G. A. Shallangwa, S. E. Abechi, In-silico screening, molecular docking, pharmacokinetics studies and design of histone deacetylase inhibitors as anti-Alzheimer agents, J. Chem. Lett. 3 (2022) 38-45.10.22034/jchemlett.2022.335742.1063.

(b) S. N. Adawara, G. A. Shallangwa, P. A. Mamza, I. Abdulkadir, In-silico modeling of inhibitory activity and toxicity of some indole derivatives towards designing highly potent dengue virus serotype 2 NS4B inhibitors, J. Chem. Lett. 3 (2022) 46-56. 10.22034/jchemlett.2022.336894.1065. (c) F. Iorhuna, A. S. Muhammad, A. M. Ayuba, A. T. Nyijime, Molecular Dynamic Simulations and Quantum Chemical Studies of Nitrogen Based Heterocyclic Compounds as Corrosion Inhibitors on Mild Steel Surface, Chem. Rev. Lett. 6 (2023) 114-127. 10.22034/crl.2023.400989.1226. (d) A. Yadav, A. Taha, Y. A. Abdulsayed, S. M. Saeed, A Density Functional Theory (DFT) Study on Adsorption of a biological active ethionamide over the Surface of a Fe-decorated porphyrin system, Chem. Rev. Lett. 6 (2023) 128-138. 10.22034/crl.2023.387354.1204.

[34] (a) M. Koohi, H. Bastami, Investigation of Ti—B nanoheterofullerenes evolved from C20 nanocage through DFT, Chem. Rev. Lett. 6 (2023) 223. 10.22034/crl.2023.392356.1222. (b) I. S. Hasan, A. A. Majhoo, M. H. Sami, A. K. O. Aldulaimi, Predicting Hydration Enthalpy of Low Molecular Weight Organic Molecules using COSMO-SAC Modeling, Chem. Rev. Lett. 6 (2023) 86-95. 10.22034/crl.2023.399189.1225. (c) K. O. Eshchanov, M. Baltaeva, Study of the interaction of sorbed silver, gold and copper ions with functional groups on hydrolyzed fibroin using Charmm22 force field calculations, Chem. Rev. Lett. 6 (2022) 161-168. 10.22034/crl.2022.335548.1159. (d) B. Mohammadi, M. R. Jalali Sarvestani, A Comparative Computational Investigation on Amantadine Adsorption on the Surfaces of Pristine, C-, Si-, and Ga-doped Aluminum Nitride Nanosheets, J. Chem. Lett. 4 (2023) 66-70. 10.22034/jchemlett.2023.388369.1107.

[35] (a) B. Ajdari, S. A. Vahed, Fullerene (C20) as a sensing material for electrochemical detection of Nortriptyline:

A theoretical study, J. Chem. Lett. 3 (2022) 164-168.10.22034/jchemlett.2023.385007.1104. (b) M. Jalali Sarvestani, Venlafaxine Interaction with Fullerene (C20): DFT Studies, J. Chem. Lett. 3 (2022) 169-173. 10.22034/jchemlett.2023.385837.1105. (c) Srinidhi, Artificial Neural Network (FFBP-ANN) Based Grey Relational Analysis for Modeling Dyestuff Solubility in Supercritical CO2 with Ethanol as the Co-Solvent, Chem. Rev. Lett. 6 (2022) 141-152. 10.22034/crl.2021.259291.1096.